Foothills seismic imaging for deep exploration in Junggar Basin — A case study

Shengtian Zhao[1], Yan Iliescu[2], Xinmin Shang[1], Houhua Teng[1], Yanguang Wang[1], and Xianhuai Zhu[2]

https://doi.org/10.1190/tle42100694.1

Abstract

Seismic imaging for deep exploration in foothills areas is currently one of the most active endeavors on land. In response to intricate challenges posed by subsurface and near-surface geology, a robust imaging workflow for land seismic data has been successfully developed. First, turning-ray tomography constrained by uphole velocity or micrologging velocity is applied to estimate a reliable near-surface velocity model by using range-limited and full-offset first arrivals. Second, a robust and seamless initial depth velocity model is constructed for prestack depth migration (PSDM) velocity model building. This model integrates the near-surface model with a legacy subsurface model. Third, tilted transverse isotropy joint turning-ray and reflection tomography, constrained by well logs and geologic interpretation, is performed to iteratively update the depth velocity model. This approach achieves improved well ties and spatial positioning of depth images from shallow to deep horizons. In the joint tomography process, 5D interpolation is employed to reduce the trace interval of common-image gathers and increase the trace numbers or common-depth point fold. As a result, the reflection tomography performs better, especially at the gap zone between the near-surface and subsurface structures. Application of the proposed methodologies and workflow to the MiQuan foothills 3D seismic data (acquired from the south rim of Junggar Basin in northwestern China) has had significant success in imaging complex subsurface structures. The final PSDM velocity model aligns with geologic expectations, and the final depth migration offers improved delineation of deep reservoirs, revealing meaningful faulting structures within a regional anticline in MiQuan. This holds significance for seismic exploration, not only in MiQuan within Junggar Basin, but also in other regions worldwide that share similar complexities in near-surface and subsurface structures.

Introduction

Seismic exploration and development in foothills areas is attractive due to favorable conditions for oil and gas accumulations. In recent years, oil producers have intensified seismic exploration efforts in foothills areas including Tarim Basin, Sichuan Basin, and Junggar Basin in China (Tian et al., 2018; Li et al., 2020),

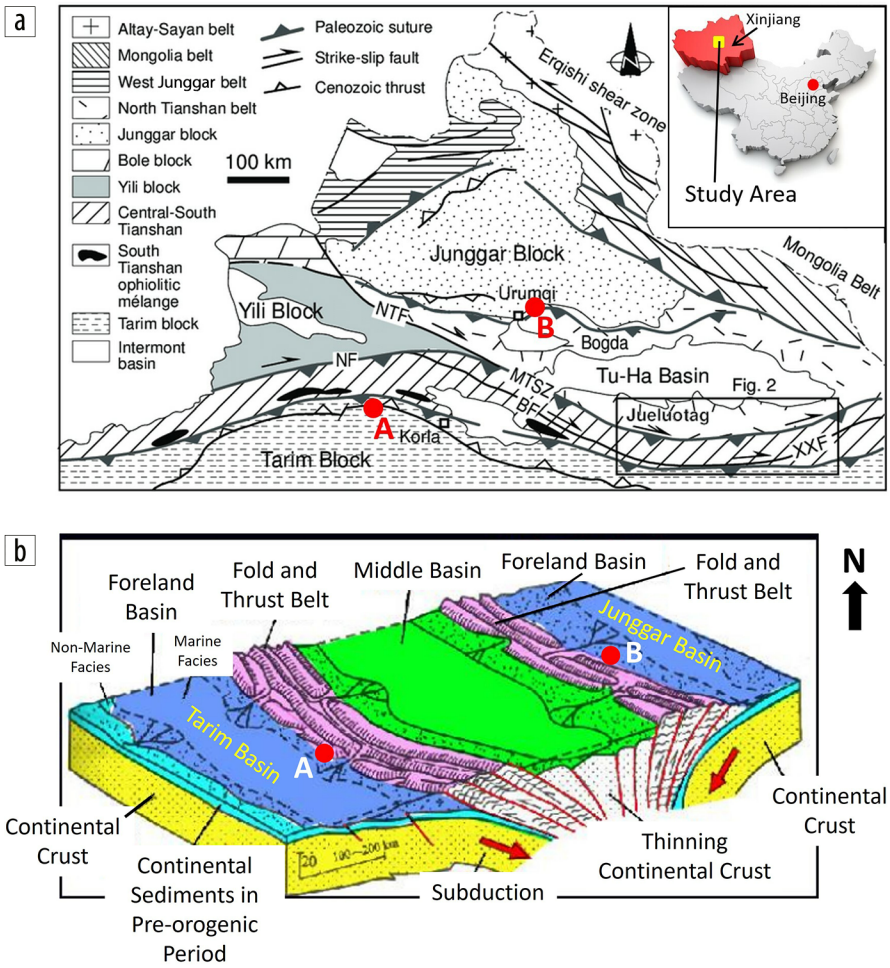

Figure 1. Regional geology. (a) Sketch map of the northern Xinjiang area in northwest China showing tectonic subdivisions of the Chinese TianShan and main bounding faults (modified from Wang et al. [2014] and Jahn [2004]). NTF = north TianShan Fault, NF = Nalati Fault, MTSZ = main TianShan shear zone, BF = Baluntai Fault, and XXF = Xingxingxia Fault. (b) The formation of the TianShan orogenic belt caused by typical horizontal movement of the crust and collision of plates or blocks (modified from Qi et al. [2006]). The Keshen structure is located at "A" in Tarim Basin, and the MiQuan structure is located at "B" in Junggar Basin.

[1]Shengli Oilfield Company, Sinopec, Shandong, China. E-mail: zhaoshengtian.slyt@sinopec.com; shangxinmin.slyt@sinopec.com; tenghouhua.slyt@sinopec.com; wangyangguang.slyt@sinopec.com.
[2]Forland Geophysical Services, Houston, Texas, USA. E-mail: yyan@forlandgeo.com; xzhu@forlandgeo.com.

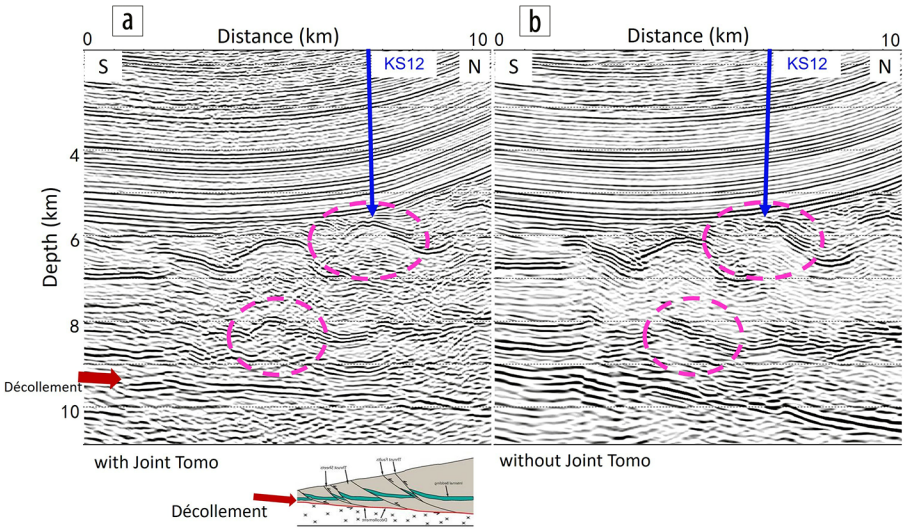

Figure 2. PSDM of Keshen structures ("A" in Figure 1) in Tarim Basin, (a) with and (b) without using joint tomography (modified from Li et al. [2020]).

as well as the Andes Mountains in South America (Gray and Zhu, 2019). The depth of exploration has deepened, and the target area now reaches 6–10 km below the surface.

However, due to complexity of near-surface and subsurface geology, imaging steeply dipping structures in foothills areas has been a persistent challenge in seismic exploration. Even within the same TianShan tectonic environment (Figure 1a), the task of imaging the Keshen structure in Tarim Basin (southern block of TianShan) differs significantly from imaging the MiQuan structure in Junggar Basin (northern block of TianShan). As a result of continent-to-continent collision, north TianShan experienced substantial uplift and evolved into thrust-nappe structures (Figure 1b). With the accumulation of fault activities, load-induced lithospheric deflection and subsidence in the foreland area in the southern margin of the Junggar block led to the formation of peripheral foreland basins.

The Keshen deep structure in Tarim Basin ("A" in Figure 1), located 6 km below the surface, can be effectively imaged (Figure 2), provided that a robust velocity model is built (Tian et al., 2018; Li et al., 2020). The décollement at approximately 10 km depth, which commonly serves as a reliable reference layer for velocity model building, becomes simpler and easier to interpret (Figure 2a). However, in MiQuan within Junggar Basin ("B" in Figure 1), situated in the northern block of TianShan, there is a noticeable absence of a prominent deep décollement that could guide the velocity update. The key issues of seismic imaging in the MiQuan area are: (1) estimating near-surface velocities and addressing static corrections, (2) constructing anisotropic depth velocity models for prestack depth migration (PSDM), and (3) performing PSDM from the true surface.

Examples of field data from MiQuan demonstrate the effectiveness of joint turning-ray and reflection tomography (Zhu et al., 2001; Tian et al., 2018) for building a tilted transverse isotropy (TTI) depth velocity model and conducting PSDM. The concept of a gap zone (often referring to an area where data for either shallow refraction tomography or deep reflection tomography are insufficient) is illustrated. Dealing with this gap zone is a crucial step in the joint tomography and foothills seismic imaging process.

It is evident that structural images in MiQuan exhibit significant improvement following joint tomography and TTI PSDM, especially within the middle to deep sections.

Study area

The MiQuan 3D survey was conducted at the southern rim of Junggar Basin. This area presents a complex exploration environment due to near-surface and subsurface structures (Song and Yu, 2012; Shang et al., 2019; Wang et al., 2021). The study area exhibits significant terrain variation, with lower elevations in the northwest and higher elevations in the southeast. The elevation ranges from 600–2200 m (Figure 3a). Figure 3b shows the surface outcrops. Beneath the surface, the study area features three sets of tectonic front structures characterized by pronounced strong structural deformation (Figure 3c). No deep décollement can be easily identified. The presence of complex shallow and deep structures, characterized by substantial formation dips and well-developed faults, significantly complicates seismic imaging efforts (Sun and Wang, 2014).

Given the characteristics of near-surface (Figures 3a and 3b) and subsurface structures (Figure 3c), as well as complexity of the seismic wavefield in MiQuan, specific methodologies in conjunction with noise-elimination approaches (Yu et al., 2017, 2020; Teng et al., 2023) have been developed to address the following velocity model building steps. The first step is estimating a reliable near-surface velocity model by using uphole velocity constrained turning-ray tomography. The second step is constructing an initial depth velocity model to serve as a good starting model for PSDM. The third step is performing TTI joint tomography (an iterative process for updating velocity and anisotropic models from the surface to deep horizons) by using anisotropic reflection tomography and PSDM.

Uphole velocity constrained turning-ray tomographic inversion

The key technology of PSDM lies in building the depth velocity model. An accurate near-surface depth velocity model must first be built to ensure a good short-wavelength static solution. This is followed by PSDM velocity model building where middle- to long-wavelength static components are taken into account. In this study, turning-ray tomography, constrained by uphole velocities, was conducted using range-limited and full-offset first arrivals (Figure 4a). The uphole velocity survey (Figure 4b), often referred to as micrologging in China, differs from conventional seismic dynamite shot-based uphole traveltime velocity measurements. These uphole surveys are designed specifically for static corrections in desert areas. They are usually acquired at spatial intervals from 0.5–1.0 km, with depths ranging from 10–200 m. After being edited and analyzed, the uphole velocities often provide localized and highly accurate information at an ultra-shallow layer (10–200 m

from the surface), which serves as effective constraints for inversions. This contributes to improved static solutions (Marsden, 1993).

Turning-ray tomography employs distinct approaches based on the offset range. For near- to middle-offset (0–4000 m) first arrivals, the finite-difference fast-marching method (FMM) (Sethian, 1996; Rawlinson and Sambridge, 2004) is adopted to construct rays. Conversely, for the full-offset (0–8000 m) first arrivals, the two-point bending ray-tracing technique (Um and Thurber, 1987) is used. Drawing on insights gained from recent foothills imaging projects, it has been observed that the tomographic inversion accuracy (when using rays calculated through the finite-difference FMM) tends to be consistently higher than that achieved with the two-point bending ray-tracing approach, particularly for the ultra-shallow layers (0–300 m). In contrast, two-point bending ray-tracing demonstrates superior accuracy and stability when compared to the FMM for the middle-deep layers (300–1500 m). This is attributed to the finite-difference FMM's precision with smaller grid sizes (less than 10 m) in the finite-difference scheme and the stability of two-point ray tracing for large model inversions, leveraging Fermat's principle to search for the shortest-traveltime path between two points.

In this study, the strengths of FMM and two-point ray-tracing methods are combined to derive an accurate near-surface velocity model. The approach begins with applying FMM, constrained by uphole velocities, to generate an accurate super-shallow (less than 300 m) near-surface velocity model. This step employs first arrivals from near-middle offsets (0–4000 m) for static corrections. Subsequently, the two-point ray-tracing technique is employed to estimate velocities of the middle-to-deep layers (300–1500 m) by using the full-offset (0–8000 m) first arrivals. Benefiting from the constraints of the FMM-derived shallow solution, the tomographic inversion, using the two-point ray-tracing method and simultaneous iterative reconstruction technique (SIRT) (e.g., Zhu et al., 1992), consistently produces accurate and reliable velocity models for the middle to deep sections (Figures 4c and 4d). Typically, ultra-shallow velocities are used for short-wavelength static corrections, while shallow to deep velocities are used for velocity model building for PSDM,

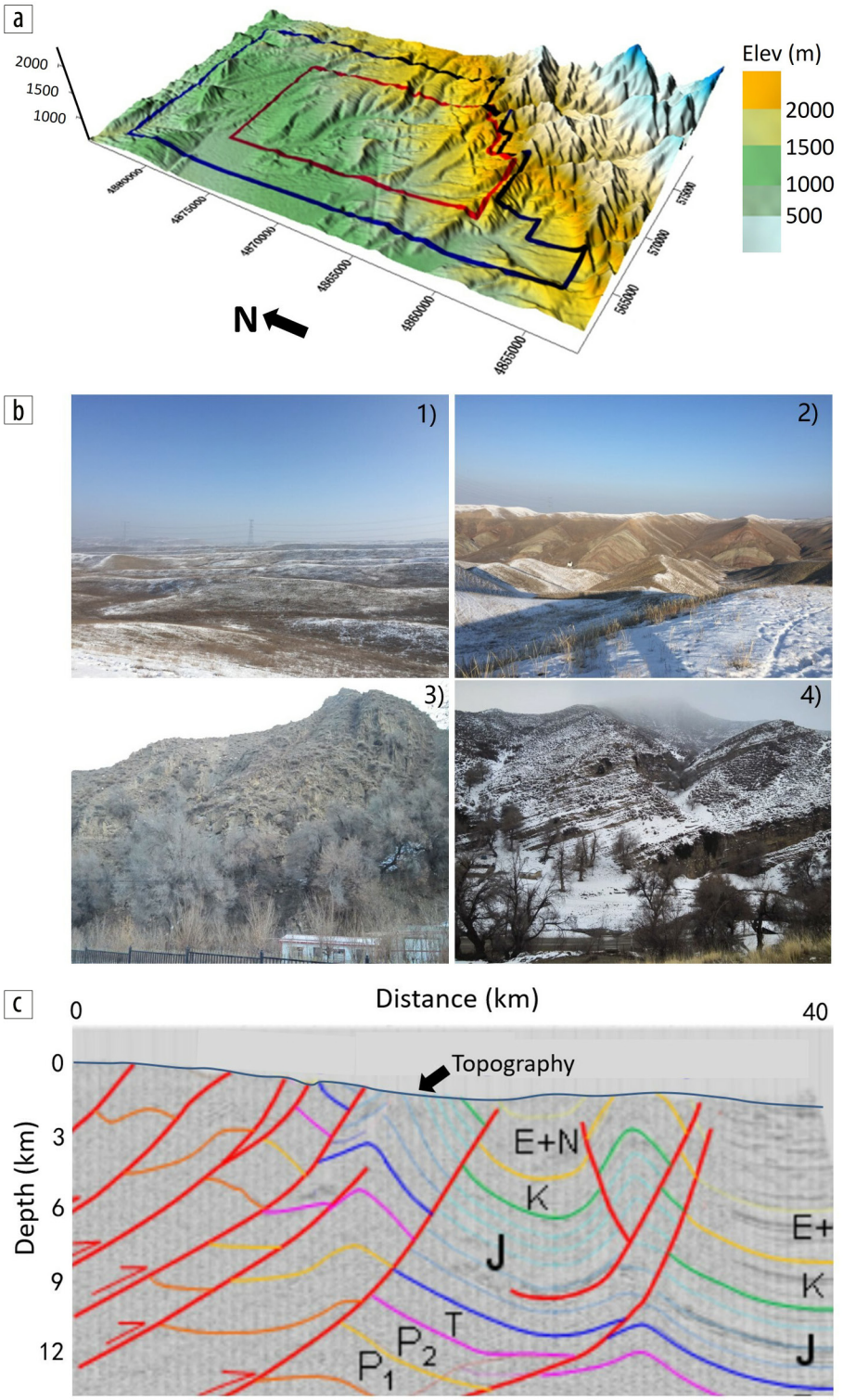

Figure 3. Near-surface and subsurface conditions in the study area. (a) Surface elevation showing rugged topography of the MiQuan 3D survey in the south rim of Junggar Basin ("B" in Figure 1). Red and blue lines show shot and receiver coverage, respectively. (b) Surface outcrops. (b1) Gobi farmland in the north. (b2) Low-velocity mountains in the north central area. (b3) Mountainous areas in the south central area. (b4) High mountains in the south. (c) Interpreted subsurface geologic features in MiQuan. P = Paleozoic, T = Triassic, J = Jurassic, K = Cretaceous, E = Eocene, and N = Neogene.

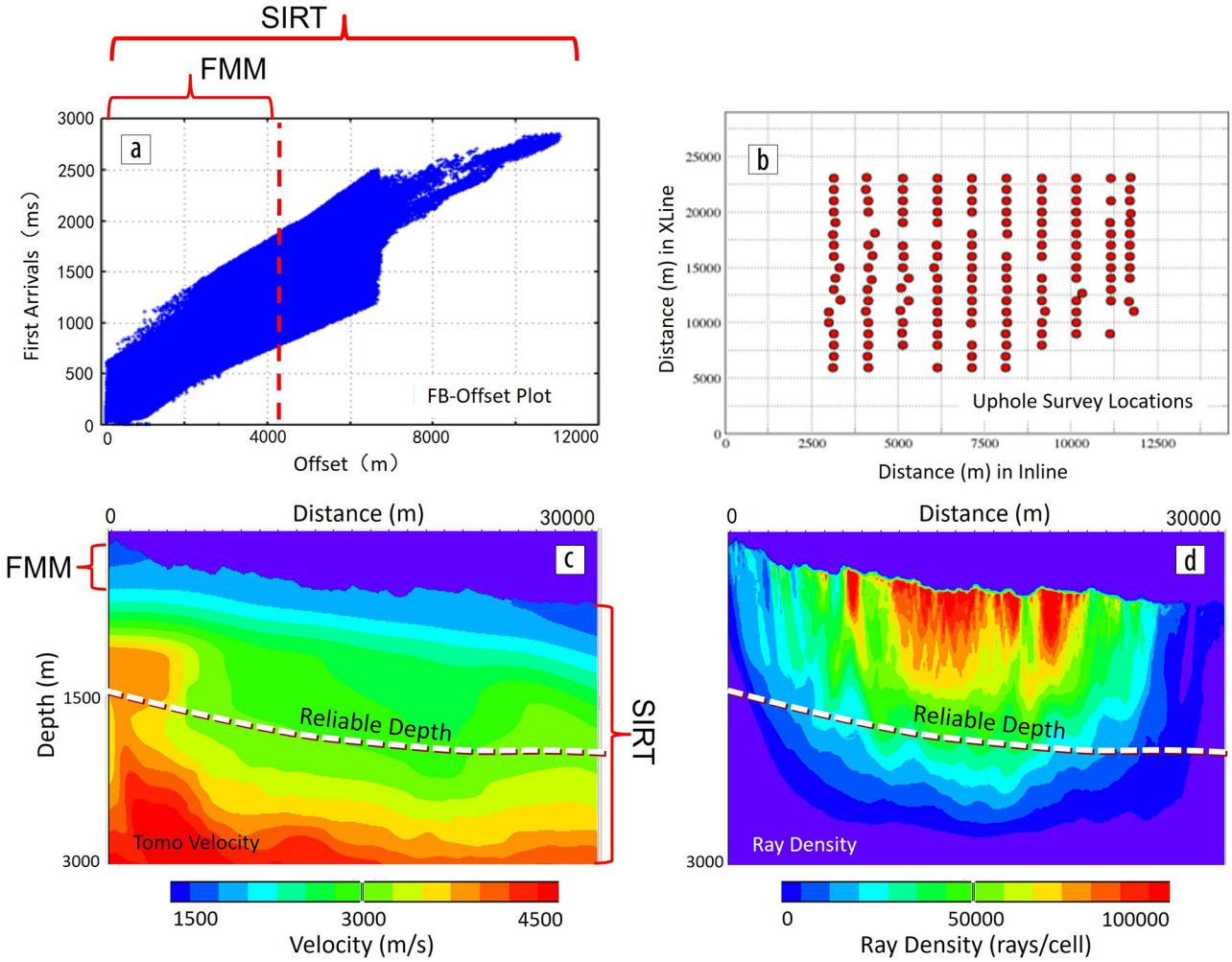

Figure 4. Shallow uphole velocity constrained turning-ray tomographic inversion. (a) MiQuan 3D first-arrival time-offset dot plot after editing. (b) Location map of 152 uphole surveys used for constrained tomography. (c) Final velocity model from constrained tomographic inversion. (d) Ray density. Near-offset (0–4200 m) first arrivals were used to estimate a super-shallow (less than 300 m) velocity model for static corrections by using the FMM ray-tracing and inversion method. Full-offset (0–9000 m) first arrivals were used to estimate a whole near-surface velocity model using the two-point bending ray-tracing and SIRT inversion method.

where the long-wavelength static component is included in the model building.

Initial depth velocity model construction

PSDM velocity model building is an iterative process, starting from shallow and progressing to deep formations. Once we have the near-surface velocity model derived from turning-ray tomography, the next step involves its integration into PSDM depth velocity model building. With a proper near-surface solution, the accuracy and efficiency of depth velocity model building can be greatly improved through application of the constrained reflection tomography (Tian et al., 2018; Li et al., 2020).

Turning-ray tomography, also known as diving-wave tomography, was proposed by Zhu et al. (1992), Stefani (1995), Zhang and Yilmaz (2005), and numerous other researchers. It serves as an effective approach to estimate the near-surface depth velocity model by using first-arrival traveltimes as input. However, the depth range achievable through reliable inversion is generally limited to ⅛ to ¼ of the maximum offset. This limitation depends on factors such as the subsurface velocity gradient and the presence of velocity reversals (Zhu et al., 1992; Li et al., 2020). Consequently, this method cannot achieve the objective of imaging deep targets.

On the other hand, reflection tomography can update deeper velocities by flattening the residual moveout of common-image gathers (CIGs). However, its ability to correct CIGs at very shallow layers is low due to limited availability of traces in the shallow section. Recognizing this, Zhu et al. (2001) present an early concept of joint tomography that integrates refraction tomography and reflection tomography. This innovative approach aims to obtain a more accurate and reliable depth velocity model for imaging deep targets.

Joint tomography requires a good starting model. To construct an effective initial depth velocity model for the joint tomography process, the near-surface velocity model from turning-ray tomography is merged or integrated vertically with a legacy subsurface velocity model. This legacy model typically comes from a relatively simple model derived from time-processed root-mean-square velocities, sonic logs, vertical seismic profiling (VSP), or prior geologic information. The reliable depth indicated by the maximum tomographic ray density (Figure 4d) at the bottom serves as the suture zone where

the near-surface and legacy subsurface velocity models merge together.

The merging process is not a simple vertical integration. Several crucial considerations, especially for the near-surface model, come into play. Addressing the edge effect of the near-surface model is one such consideration. The ray-density plot in Figure 4d shows a boat shape. This is a consequence of turning rays requiring a certain distance for downward and upward wave propagation in accordance with Snell's law, preventing them from returning vertically to the surface. Therefore, before merging, a series of processing steps is essential to render the near-surface velocity model suitable for PSDM depth velocity model building such as velocity editing to eliminate anomalies, smoothing, and edge extension to ensure the velocity model aligns with geologic features (Figure 5).

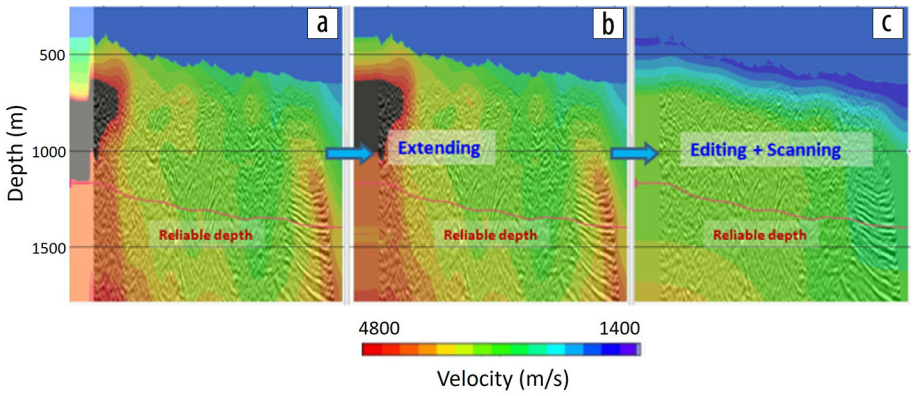

Figure 5. Editing of the near-surface velocity model used for joint tomography. (a) Original near-surface velocity model estimated by turning-ray tomography. (b) After edge extension. (c) After editing and percentage scanning.

At the transition zone of integration between the near-surface and legacy subsurface velocity models, tapering is typically applied to prevent abrupt velocity changes. Figure 6 shows the merged initial depth velocity model. The initial depth velocity model clearly conforms to the overall geologic structure. The background velocity field exhibits notable smoothness and simplicity, free from velocity anomalies. This merged, coherent, and seamlessly blended velocity model will serve as the initial depth velocity model for PSDM velocity model building using joint tomography.

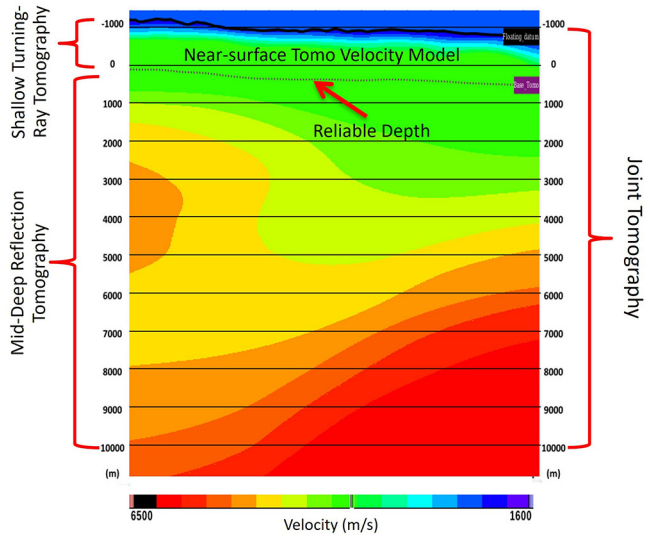

Figure 6. Construction of initial depth velocity model for joint tomography.

TTI joint tomography

Reflection tomography is a global optimization. At early stages of updating the velocity model, inaccuracies are typically more pronounced in deeper areas compared to shallower areas. To prevent propagation of errors to the shallow areas, these sections are masked and unchanged during the early stages of iterations in the joint tomography (Figure 6). Following several iterations of reflection tomography, the errors in deeper areas gradually diminish. To account for the errors associated with first-arrival picking and model merging, the later stages of iterations enable reflection tomography to concurrently update shallow and deep areas (Figure 6) (Tian et al., 2018).

The TTI joint tomography workflow is illustrated in Figure 7. This approach employs well-log data, tops, and interpreted seismic horizons as constraints. The velocity and TTI parameters (delta [δ], epsilon [ε], dip, and azimuth) undergo iterative updates through joint tomography to achieve improved well ties and reasonable spatial positioning of the image. The δ model is typically determined through well-tie analysis by comparing geologic markers to interpreted depth horizons. Updates to the δ model can be performed with mis-tie tomography (Figure 7), a technique that estimates δ parameters by minimizing mis-ties. The ε values for layers can be estimated based on overall event flatness, especially at far offsets. The dip and azimuth in the TTI layers are derived from the dip and azimuth of the horizons at the layer boundaries of depth-migrated images.

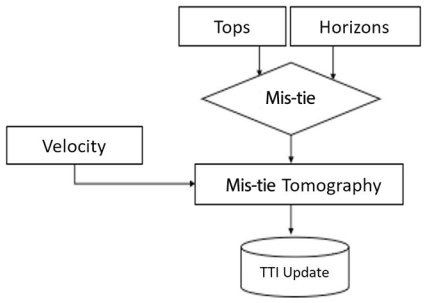

Figure 7. TTI joint tomography workflow.

At the gap zone between the shallow refraction tomography and deep reflection tomography, the number of traces in a CIG is often limited, and 5D interpolation can improve the robustness of reflection tomography in the zone. As depicted in Figure 8, prior to applying 5D interpolation, there are a mere seven traces available for a specific event at the gap zone, which does not give sufficient curvature for effective reflection tomography (Figure 8b). Subsequent to the interpolation process, 18 traces are reconstructed, resulting in more clearly defined curvature and improved performance for reflection tomography (Figure 8b).

Application to MiQuan 3D data

The dominant maximum offset of MiQuan 3D is 7000 m, and some offsets reach 10,000 m (Figure 4a). Constrained by 152 uphole velocity survey data (Figure 4b), the near-surface model from turning-ray tomography is shown in Figure 4c, and ray density from turning-ray tomography is shown in Figure 4d. The reliable depth (down from the surface) is about 1500 m, which provides a good shallow velocity solution for subsequent joint tomography. When performing turning-ray tomography, the uphole velocity constraint helps inversion further improve the accuracy of the super-shallow velocity model (0–50 m) (Jin et al., 2020). However, it is important to note that improper utilization of uphole velocity data can lead to a phenomenon known as the bull's-eye effect. To prevent occurrence of the phenomenon and enhance stability, a viable strategy involves constructing a 3D velocity volume through spatial and azimuthal interpolation of uphole velocities. This volume is then utilized as a constraint during the turning-ray inversion process, thereby improving accuracy and reliability. If the depth of the majority of uphole surveys is 10–20 m or less, constrained turning-ray tomography is not recommended. This is due to the typical depth increment used by turning-ray tomography, which is about 10 m.

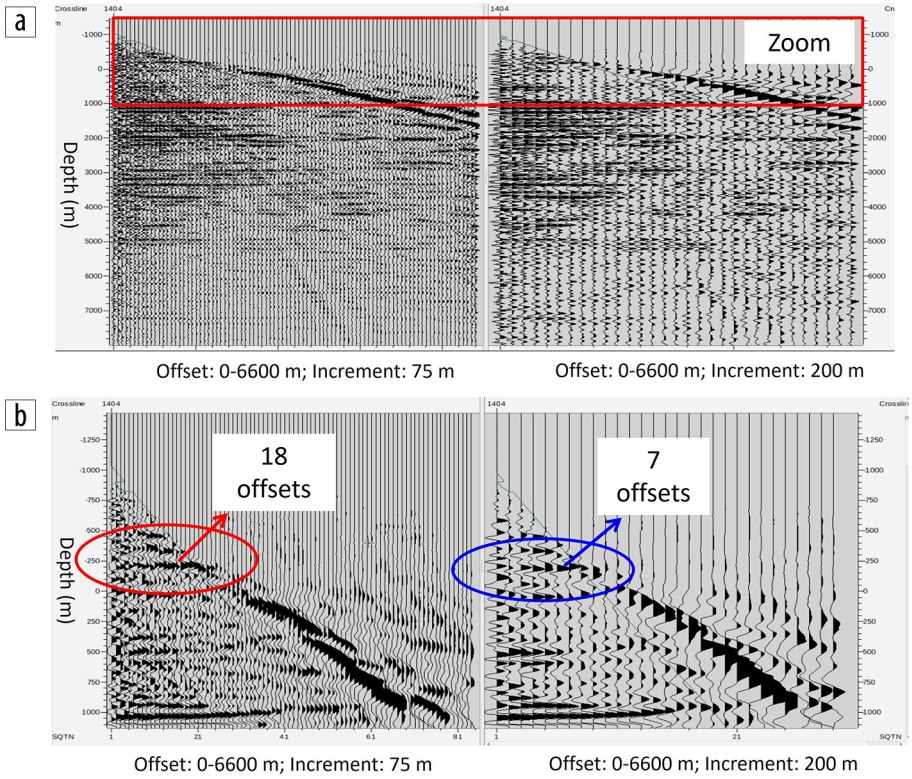

Figure 8. Gap zone before and after 5D interpolation. (a) CIG from MiQuan 3D after 5D interpolation and before 5D interpolation. The shallow zoomed portion is shown in (b). The gap zone between the near-surface and subsurface structures is highlighted by circles. The number of traces for a specific event in the CIG has been increased from seven to 18 after interpolation.

Figure 9 shows the TTI anisotropic parameter models along a specific inline, with the velocity representing the layer velocity perpendicular to the formation. δ and ε govern the vertical and lateral corrections for seismic imaging, respectively. Additionally, dip and azimuth are calculated from the depth-migrated seismic stack volume, and these values are directly tied to the underlying geologic features.

Figure 10 shows the comparison of PSDM gathers using the initial model and the final model updated by TTI joint tomography. Notably, following iterative updates, seismic events within the final PSDM gathers, from shallow to deep and from near to far offsets, have been reasonably corrected and flattened.

Figure 11 shows a comparison of the newly processed PSDM stack section and the legacy PSDM stack section. Evidently, the application of joint TTI tomography has notably enhanced PSDM images. The prominent structures within the zone of interest (indicated by

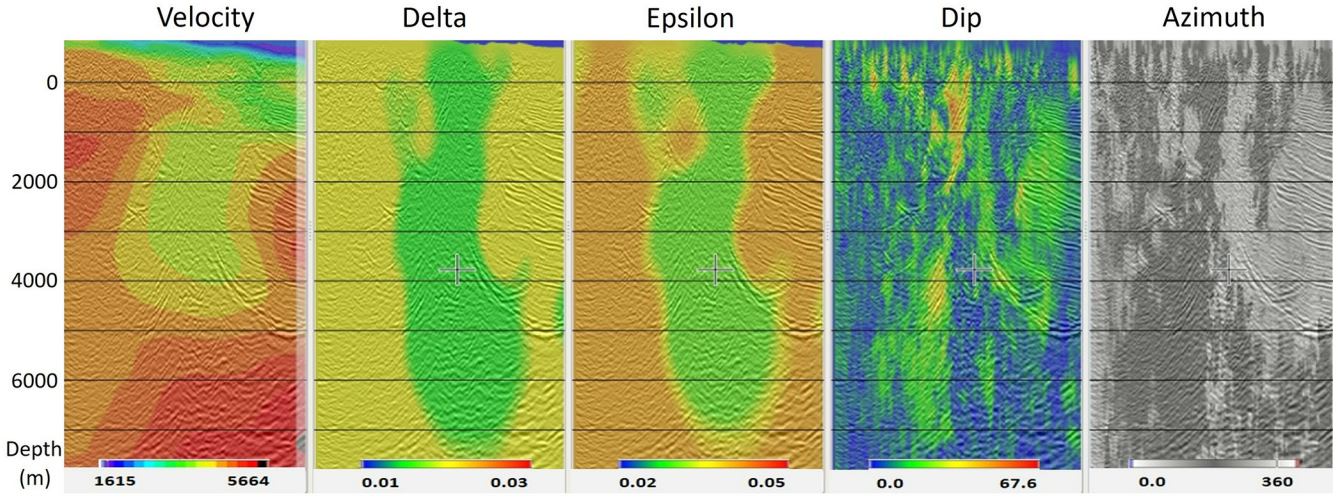

Figure 9. Updated TTI parameter models.

arrows in Figure 11a) are characterized by enhanced geologic simplicity and coherence, ultimately contributing to a more accurate structural interpretation.

Conclusions

This paper outlines a depth velocity model building approach through joint tomography for PSDM imaging in complex areas. The effectiveness of the approach has been validated by its application to MiQuan 3D field data acquired from Junggar Basin. It provides new insight into seismic exploration in foothills areas worldwide.

The paper introduces two forms of joint tomography. The first focuses on near-surface depth velocity model building for static corrections and initial model construction for PSDM. The second involves global optimization of the depth velocity model from shallow to deep sections for prestack depth migration. The main observations and conclusions are as follows.

Joint near-surface velocity model building, combining FMM and two-point bending ray-tracing techniques for turning-ray tomographic inversions, proves practical for static corrections and PSDM in foothills areas. The process entails FMM inversion, using first arrivals from the near to middle offsets, to estimate an ultra-shallow (usually less than 300 m) velocity model, ensuring effective static corrections. Subsequently, two-point ray tracing, aided by SIRT iterative nonlinear inversion using full-offset first arrivals, was carried out to maximize the reliable depth of the near-surface solution. Short-wavelength static corrections are beneficial for time-domain data conditioning, while middle- to long-wavelength static components should be integrated into the depth velocity model building for PSDM.

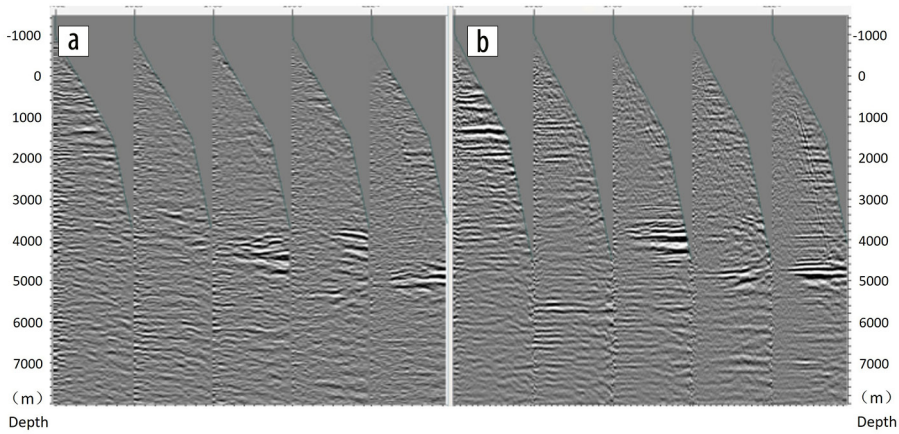

Figure 10. PSDM gathers using (a) the initial velocity model and (b) final velocity model from TTI joint tomography.

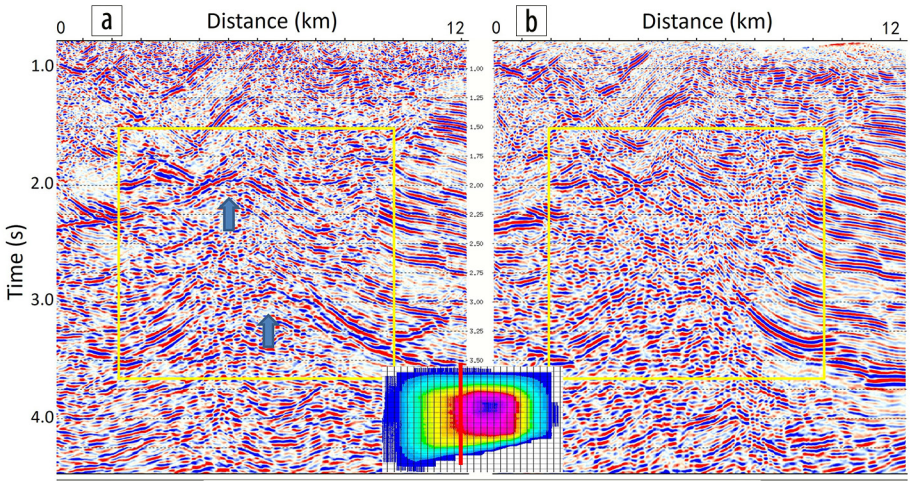

Figure 11. PSDM stack (converted to time) comparison. (a) Reprocessed PSDM stack by TTI joint tomographic inversion. (b) Legacy PSDM stack without joint tomographic inversion. Arrows and yellow outlines show the targets of interest. Red line on the fold map shows the seismic profile location.

During the uphole velocity constrained inversion, stability must be taken into account to prevent occurrence of a bull's-eye effect in a 3D volume. When using VSP to calibrate tomographic inversion velocity, careful selection of reliable VSP data is crucial to avoid misleading velocity estimations. The trustworthy depth of the near-surface velocity model estimated from turning-ray tomography spans about ⅛–¼ of the maximum offset, depending on the near-surface velocity gradient. Hence, full-offset first arrivals should be employed to reach the maximum reliable depth of the near-surface velocity model.

Joint turning-ray (refraction) and reflection tomography emerges as a cutting-edge technology for imaging deep reservoirs in land and foothills areas. Employing integration TTI joint tomography initially stabilizes the shallow depth velocity model to rectify significant subsurface velocity errors, primarily in the middle and deep layers. Subsequently, it broadens the scope for shallow model updating on a global scale, facilitating iterative optimization of the depth velocity model from shallow to deep layers. The rationale behind residual error updates in the shallow layers stems from inherent errors in first-arrival picking, whether it is automatic picking, artificial intelligence (AI) picking, or manual picking in complex surface areas, particularly in foothills areas. This global optimization approach ensures the attainment of an overall depth velocity model with enhanced accuracy.

Future direction for exploration includes full-waveform inversion (FWI). FWI faces challenges in land and foothills areas when modeling observed data, which contain diverse wave types such as P- and S-waves, scattering and backscattering noise, guided waves, converted waves, and multiples. Addressing this challenge may involve eliminating certain types of waves to minimize the difference between observed and modeled waveforms. Additionally, there is potential for advancing toward a streamlined one-step joint tomographic inversion process. Presently, joint tomographic inversion typically involves partitioning into two or more steps, demanding processors to possess specific expertise. Lastly, application of AI holds promise. It is expected that AI could improve the performance of FWI and one-step joint tomography. TLE

Acknowledgments

We thank Allen Bertagne, Junru Jiao, Kun Xu, and Bin Yang for constructive discussions. Uphole velocity constrained tomography was implemented by Kun Xu. High-resolution graphics were created by Qing Ma. Comments and suggestions from Chengbo Li, Chao Wang, and two anonymous reviewers are very much appreciated. We also thank Sinopec Shengli Oilfield Company and Forland Geophysical Services for permission to publish the results.

Data and materials availability

Data associated with this research are confidential and cannot be released.

Corresponding author: yyan@forlandgeo.com

References

Gray, S., and X. Zhu, 2019, Foothills seismic imaging challenges: Past, present and future: 2nd Foothill Exploration Workshop, SEG, Expanded Abstracts, https://doi.org/10.1190/FEW2019-01.1.

Jahn, B.-M., 2004, The Central Asian orogenic belt and growth of the continental crust in the Phanerozoic, *in* J. Malpas, C. J. N. Fletcher, J. R. Ali, and J. C. Aitchison, eds., Aspects of the tectonic evolution of China: Geological Society of London, 73–100, https://doi.org/10.1144/GSL.SP.2004.226.01.05.

Jin, C., Y. Wang, X. Shang, Q. Cui, and D. Wang, 2020, Near-surface velocity modeling based on micro-log and azimuth-weighted interpolation: Oil Geophysical Prospecting, **55**, no. 2, 257–265, https://doi.org/10.13810/j.cnki.issn.1000-7210.2020.02.004.

Li, Y., X. Zhu, G. Peng, L. Liu, and W. Duan, 2020, Novel strategies of complex foothills seismic imaging — Part 1: Mega-near-surface velocity estimation: Interpretation, **8**, no. 3, T651–T665, https://doi.org/10.1190/INT-2019-0204.1.

Marsden, D., 1993, Static corrections — A review, Part 1: The Leading Edge, **12**, no. 1, 43–49, https://doi.org/10.1190/1.1436912.

Qi, J. F., Y. P. Xia, and Q. Yang, 2006, Structural analysis of oilfields: Petroleum Industry Press.

Rawlinson, N., and M. Sambridge, 2004, Wave front evolution in strongly heterogeneous layered media using the fast marching method: Geophysical Journal International, **156**, no. 3, https://doi.org/10.1111/j.1365-246X.2004.02153.x.

Sethian, J. A., 1996, A fast marching level set method for monotonically advancing fronts: Proceedings of the National Academy of Sciences of the United States of America, **93**, no. 4, 1591–1595, https://doi.org/10.1073/pnas.93.4.1591.

Shang, X., Y. Wang, Q. Chui, C. Jin, C. Zhao, H. Teng, and S. Zhao, 2019, Research on fine near-surface modeling in south foothill belt of Junggar Basin: Progress in Geophysics, **34**, no. 5, 1887–1892, https://doi.org/10.6038/pg2019CC0287.

Song, G., and S. Yu, 2012, Progress and strategy of the seismic exploration in foothill area: Geophysical Prospecting for Petroleum, **51**, no. 6, 539–547.

Stefani, J. P., 1995, Turning-ray tomography: Geophysics, **60**, no. 6, 1917–1929, https://doi.org/10.1190/1.1443923.

Sun, Z., and Y. Wang, 2014, Structural analysis and modeling in Miquan area of the western margin of the Bogda Mountain, Xinjiang: Geoscience, **28**, no. 2, 300–307.

Teng, H., J. Jiao, X. Shang, Y. Wang, S. Zhao, G. Yan, B. Yang, and X. Zhu, 2023, Two-dimensional complex wavelet transform for linear noise attenuation and image decomposition: Journal of Geophysics and Engineering, **20**, no. 3, 474–482, https://doi.org/10.1093/jge/gxad022.

Tian, J., P. Gengxin, J. Jiao, G. Yan, and X. Zhu, 2018, Integrated turning-ray and reflection tomography for velocity model building in foothill areas: Interpretation, **6**, no. 4, SM63–SM70, https://doi.org/10.1190/INT-2018-0005.1.

Um, J., and C. Thurber, 1987, A fast algorithm for two-point seismic ray tracing: Bulletin of the Seismological Society of America, **77**, no. 3, 972–986, https://doi.org/10.1785/BSSA0770030972.

Wang, B., D. Cluzel, B. Jahn, L. Shu, Y. Chen, Y. Zhai, Y. Branquet, L. Barbanson, and S. Sizaret, 2014, Late Paleozoic pre- and syn-kinematic plutons of the Kangguer-Huangshan shear zone: Inference on the tectonic evolution of the eastern Chinese north Tianshan: American Journal of Science, **314**, no. 1, https://doi.org/10.2475/01.2014.02.

Wang, Y., X. Shang, S. Zhao, H. Teng, G. Yan, and X. Zhu, 2021, Joint tomography for foothills seismic imaging: Oil Geophysical Prospecting, 782–791, https://doi.org/10.13810/j.cnki.issn.1000-7210.2021.04.011.

Yu, Z., R. Abma, J. Etgen, and C. Sullivan, 2017, Attenuation of noise and simultaneous source interference using wavelet denoising: Geophysics, **82**, no. 3, https://doi.org/10.1190/geo2016-0240.1.

Yu, Z., R. Johnston, J. Etgen, and A. Reitz, 2020, A nonlinear solution to 3D seismic data conditioning using trained dictionaries: Geophysics, **85**, no. 5, V397–V406, https://doi.org/10.1190/geo2019-0557.1.

Zhang, J., and O. Yilmaz, 2005, Near-surface corrections for complex structure imaging: 75th Annual International Meeting, SEG, Expanded Abstracts, 2566–2568, https://doi.org/10.1190/1.2148247.

Zhu, X., D. P. Sixta, and B. G. Angstman, 1992, Tomostatics: Turning-ray tomography + static corrections: The Leading Edge, **11**, no. 12, 15–23, https://doi.org/10.1190/1.1436864.

Zhu, X., K. Wyatt, and A. Lau, 2001, Turning-ray tomography and tomostatics: Presented at the 71st Annual International Meeting, SEG.